


PAPER • OPEN ACCESS

Fractal boundaries in chaotic hamiltonian systems

To cite this article: R L Viana *et al* 2017 *J. Phys.: Conf. Ser.* **911** 012002

View the [article online](#) for updates and enhancements.

Related content

- [Fractal structures in the Hénon-Heiles Hamiltonian](#)
R. Barrio, F. Blesa and S. Serrano
- [Bifurcations and safe regions in open Hamiltonians](#)
R Barrio, F Blesa and S Serrano
-  [-functions and Hamiltonian systems](#)
S Yu Shorina

Fractal boundaries in chaotic hamiltonian systems

R L Viana¹, A C Mathias¹, F A Marcus¹, T Kroetz² and I L Caldas³

¹ Departamento de Física, Universidade Federal do Paraná, Curitiba, Paraná, Brazil

² Departamento de Física, Universidade Tecnológica Federal do Paraná, Pato Branco, Paraná, Brazil

³ Instituto de Física, Universidade de São Paulo, São Paulo, São Paulo, Brazil

E-mail: viana@fisica.ufpr.br

Abstract. Fractal structures are typically present in the dynamics of chaotic orbits in non-integrable open Hamiltonian systems and result from the extremely complicated nature of the invariant manifolds of unstable periodic orbits. Exit basins, the set of initial conditions leading to orbits escaping through a given exit, have very frequently fractal boundaries. In this work we analyze exit basin boundaries in a dynamical system of physical interest, namely the motion of charged particles in a magnetized plasma subjected to electrostatic drift waves, and characterize in a quantitative way the fractality of these structures and their observable consequences, as the final-state uncertainty.

1. Introduction

In open chaotic hamiltonian systems there are initial conditions generating orbits which eventually exit from the system. Suppose there are two or more different ways in which an orbit can exit from the system. We define the exit (or escape) basin as the set of initial conditions in a certain phase-space region leading to orbits escaping through a given exit [1]. In particular we are interested in characterizing the boundary between these exit basins, which is often fractal and thus presents final-state sensitivity: a slight perturbation of some initial condition may lead to an orbit escaping through a different exit, impairing our capacity of predict the future outcome of the system [2, 3].

This problem has various applications in many fields. In celestial mechanics for example, Contopoulos and coworkers [4, 5] has studied the escape of stars from a galaxy using a paradigm hamiltonian such that, for energies larger than a critical value, there exists channels whereby orbits may escape to infinity. More recently Aguirre *et al.* have studied the exit basins of such a problem using the Hénon-Heiles hamiltonian [6].

Other field in which exit basins have been intensively studied in recent years is plasma physics. The escape of magnetic field lines in a magnetically confined fusion plasma with destroyed magnetic surfaces presents fractal exit basins [7, 8]. Another problem in which such fractal structures appear is the charged particle motion in a magnetized plasma under electrostatic drift waves [9], which is a relevant scenario in the study of plasma turbulence in the plasma edge in a tokamak [10, 11].

In this paper we present some results on the characterization of exit basins in the abovementioned problem of particle motion under two drift waves, which is hamiltonian but generally nonintegrable. The existence of a chaotic, area-filling orbit in phase space, and its



corresponding homoclinic tangle, is ultimately responsible for the fractality of exit basins [12]. We characterize the latter by computing the box-counting dimension of the exit basin boundaries, using the uncertainty fraction method [2] and also by calculating the basin entropy and basin boundary entropy, two concepts recently developed by Daza et al. [13].

This paper is organized as follows: in Section II we introduce the physical system to be considered, as well as the chaoticity of particle motion we focus on. Section III deals with the subject of exit basins and the characterization of their fractality. The last Section is devoted to our Conclusions.

2. Model

It is well-known that the motion of a particle of mass m and charge e in a uniform magnetic field B_0 , also called gyration, is a combination of a circular motion of radius mv/eB_0 on the plane perpendicular to \mathbf{B} and a uniform motion along \mathbf{B} . The motion of particle's guiding center suffers a drift when an electric field $\mathbf{E} = -\nabla\Phi$ is present. The velocity of such $\mathbf{E} \times \mathbf{B}$ is given by [14]

$$\mathbf{v} = -\frac{\nabla\Phi \times \mathbf{B}}{B^2}. \quad (1)$$

In our discussion we neglect all energy dissipation caused by, e.g. collisions between particles with energy and momentum exchange. If such effects were to be taken into account the system would become dissipative, with a completely different dynamics. However, the effect of such collisions can be neglected if the collisional frequency is small enough.

Factoring out the gyration, we can focus on the drift motion of the charged particles with a velocity \mathbf{v} , whose components satisfy canonical equations

$$\frac{dx}{dt} = -\frac{\partial H}{\partial y}, \quad \frac{dy}{dt} = \frac{\partial H}{\partial x}, \quad (2)$$

where the Hamiltonian is $H(x, y, t) = \Phi(x, y, t)/B_0$. In the following, all variables have been suitably nondimensionalized.

The electric potential has an equilibrium part $\Phi_0(x)$ corresponding to a radial electric field and a perturbation caused by two electrostatic drift waves with amplitudes $A_{1,2}$, frequencies $\omega_{1,2}$ and wave vectors $\mathbf{k}_{1,2}$, in which, by a canonical transformation, leads to the following Hamiltonian [15]

$$H(x, y, t) = \Phi_0(x) - u_1 x + A_1 \sin(k_{x1}x) \cos(k_{y1}y) + A_2 \sin(k_{x2}x) \cos[k_{y2}(y - ut)], \quad (3)$$

where $u_{1,2} = \omega_{1,2}/k_{y1,2}$ are the phase velocities of the drift waves and $u = u_2 - u_1$. We suppose that a stationary wave pattern along the radial distance x and a travelling wave along the poloidal direction y , such that the wave numbers are chosen as $k_x = n\pi/L_x$ and $k_y = 2\pi m/L_y$, where m and n are suitably chosen positive integers and $L_{x,y}$ are characteristic lengths [9]. We suppose a uniform electric field applied in the radial direction of the tokamak, such that $\Phi_0 = E_0 x$. In this model we neglect some collective effects in the plasma and consider it simply a collection of non-interacting charged particles. Within this approximation, the interaction of the confined plasma with the electric and magnetic fields does not lead to collective effects, such as mechanical or magnetohydrodynamical waves.

The canonical equations (2) were numerically integrated for the Hamiltonian (3), and a Poincaré map was taken after considering only those values of (x, y) at times equal to an integer multiple of the period $T = 20\pi$. We choose A_2 (amplitude of the second wave) as the perturbation strength. The case $A_2 = 0$ represents an integrable system, and the particle motion is bounded within 4×4 cells limited by the separatrices emanating from the hyperbolic

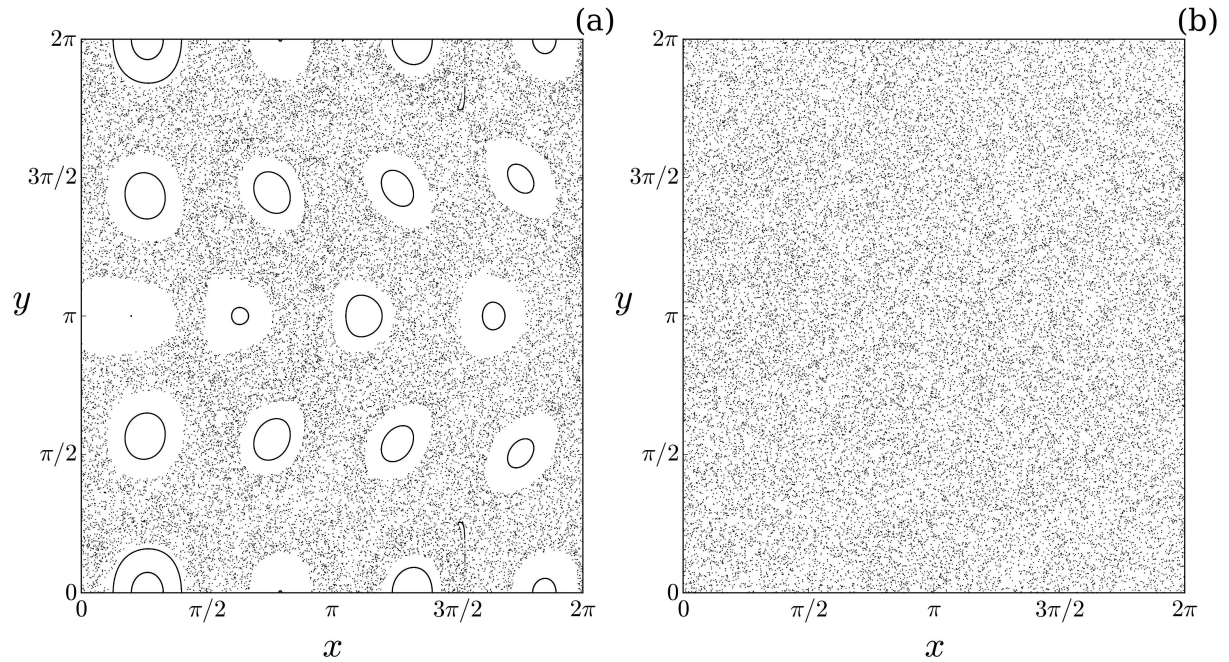


Figure 1. Phase portrait for the Poincaré map for $\omega_1 = \omega_2 = 0.2$, $k_{x1} = k_{y1} = 2.0$, $k_{x2} = \sqrt{3}$, $k_{y2} = 1.0$, $u = 0.1$, $A_1 = 1.0$ and (a) $A_2 = 0.8$, (b) $A_2 = 1.5$.

fixed points of the Poincaré map. In the interior of each cell there are closed curves orbiting around the elliptic fixed points.

In Fig. 1 we show two phase portraits for the Poincaré map obtained with different values of the perturbation intensity. For the case of smaller perturbation [Fig. 1(a)] the system integrability is broken, and the separatrices of the cells give place to a localized area-filling chaotic orbit, which is considerably enlarged as the perturbation is increased, practically engulfing all the remnant islands [Fig. 1(b)].

3. Exit basins

The chaotic orbits depicted in Fig. 1(a) and (b) allow particle transport over all the available phase space region. Since the left-hand boundary of this region coincides with the tokamak wall ($x = 0$) those particles hitting this line can be considered as effectively lost, due to many plasma-wall processes like sputtering. In order to investigate the distribution of particle escape through this wall we will divide it into two congruent segments: $\mathbf{A} = \{x = 0, 0 < y \leq \pi\}$ and $\mathbf{B} = \{x = 0, \pi < y \leq 2\pi\}$.

The next step is to cover the phase space region in Fig. 1 with a fine mesh of points and, considering each mesh point an initial condition (x_0, y_0) we iterated the Poincaré map and wait until the ensuing orbit escape through the wall at $x = 0$. If the trajectory has escaped through exit \mathbf{A} (\mathbf{B}) the corresponding initial condition is painted green (red). The sets of green and red pixels are thus numerical approximations of the basins of exits \mathbf{A} and \mathbf{B} , respectively. The white pixels stand for initial conditions that do not escape, since they are inside the periodic islands. The results are depicted in Fig. 2(a) and (b) for the same parameter values used in the phase portraits of Fig. 1(a) and (b).

A visual inspection of Figs. 2(a) and (b) shows that the size of the green basin is considerably

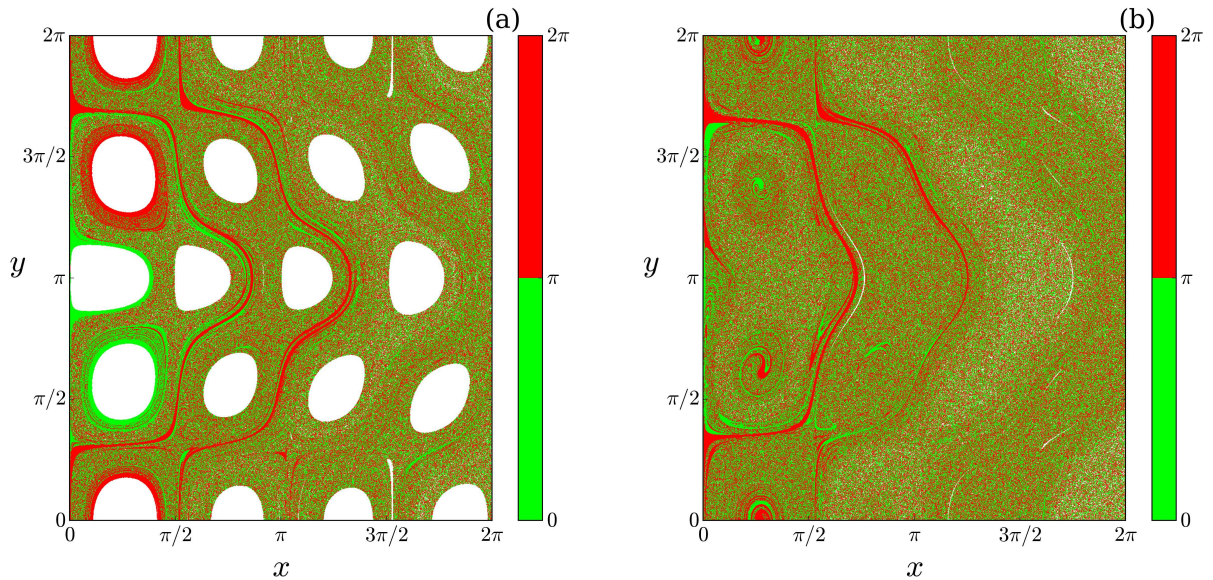


Figure 2. Basins of the exits $\mathbf{A} = \{x = 0, 0 < y \leq \pi\}$ (green pixels) and $\mathbf{B} = \{x = 0, \pi < y \leq 2\pi\}$ (red pixels) for the same parameters of Fig. 1, and (a) $A_2 = 0.8$, (b) $A_2 = 1.5$.

smaller than for the red basin. This means that most initial conditions escape through exit \mathbf{B} , i.e. the escape pattern is strongly nonuniform. The reason for this behavior is the structure of invariant manifolds (stable and unstable) that cross themselves in an infinite number of homoclinic and heteroclinic points. Since the manifolds have an extremely involved behavior, the resulting meanders act as escape channels, through which the phase space trajectories are directed to escape towards $x = 0$.

When two exit basins are intertwined the way shown in Fig. 2, it is typically found that their common boundary is fractal. In order to check this fact we computed the box counting dimension of this boundary using the uncertainty fraction technique [2, 3]. We know that an initial condition is known up to a given uncertainty ε , represented by a ball of radius ε centered at that initial condition. If this ε -ball intercepts the basin boundary, we cannot be sure to which exit that initial condition will evolve to one. In this case we say that the initial condition is ε -uncertain.

The fraction of uncertain initial condition scales with the uncertainty as $f(\varepsilon) \sim \varepsilon^\alpha$, where $0 < \alpha < 1$ is called the uncertainty exponent. The latter is related to the box-counting boundary dimension D_0 by $\alpha = 2 - D_0$, in a two-dimensional phase space [2]. If the boundary is a smooth curve, then $\alpha = 1$ and $D_0 = 1$, whereas $\alpha < 1$ is for a fractal boundary. Using this technique we found that the box-counting dimension of the boundary between red and green basins in Fig. 2(a) and (b) is $D_0 = 1.945 \pm 0.002$ and $D_0 = 1.956 \pm 0.002$, respectively. Hence the basin boundary dimension has increased with the perturbation, and it approaches 2.0, which would mean an area-filling curve.

The box-counting dimension, while useful to characterize the fractality of the exit basin boundary, do not give information about the degree in which these basins are intertwined. A more convenient measure for this purpose is the basin entropy introduced by Daza *et al.* [13]. We start by covering a given region of the phase space by a grid of 1000×1000 points of each basin, distributed inside 4×10^4 boxes. For each grid point, a maximum of 1.5×10^4 stroboscopic map points were obtained, and excluding those initial conditions that have not escaped during

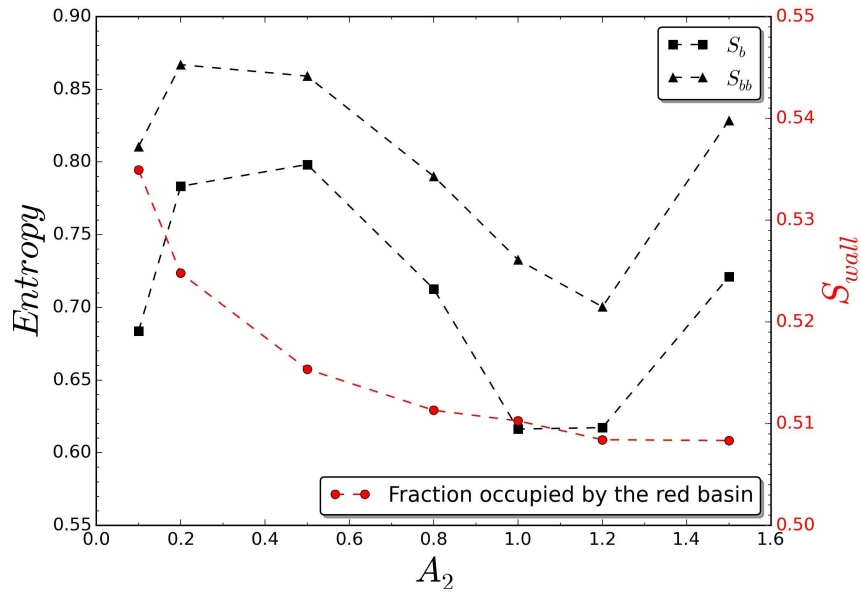


Figure 3. Basin entropy and basin boundary entropy for the case of two exits [see Fig. 2] as a function of the second wave amplitude. We also plot the fraction occupied by the red basin.

that time.

Let n_1 be the number of points of the box corresponding to the exit 1, and n_2 to exit 2. For each box we obtained the probabilities $p_1 = n_1/(n_1 + n_2)$ and $p_2 = n_2/(n_1 + n_2)$, and we apply the Gibbs entropy definition for each box [13]:

$$S = - \sum_{i=1}^2 p_i \log_2(p_i). \quad (4)$$

The basin entropy S_b is the sum of the values of S for those boxes such that all the initial conditions escape, divided by the number of boxes N_b for which all initial conditions escape. The boundary basin entropy S_{bb} was obtained analogously, but excluding those boxes for which either $p_1 = 0$ or $p_2 = 0$, i.e., there were considered only the boxes that have at least one boundary in their interior.

If there were a single exit the basin entropy would vanish, meaning zero final-state uncertainty. On the other hand, if the two exits are equiprobable, in the sense that their basins are of comparable sizes and densely intertwined, the maximum value of the basin entropy would be $S_b = \log_2 2 = 1$, i.e. a completely randomized basin structure.

We show in Fig. 3 the values of the basin entropy S_b and the basin boundary entropy S_{bb} for the two exits as a function of the second wave amplitude A_2 . It is also plotted the fraction S_{wall} occupied by the (red) basin of the exit **B** (the fraction of the green basin is $1 - S_{wall}$). The values of S_{wall} are slightly higher for weak perturbation (about 53%) and tend to 51% for strong perturbation. This fact is exemplified by Fig. 2(a) and (b), in which the green and red basins are more intertwined for stronger perturbation. We observe that the values of S_b fluctuate between 0.68 and 0.80 for the range of perturbation considered, meaning that the basins are mixed together in a very complicated way for all considered values of the perturbation strength A_2 .

4. Conclusions

The dynamics in chaotic orbits of non-integrable open Hamiltonian systems is strongly influenced by fractal structures coming from the complicated intersections between stable and unstable invariant manifolds of unstable periodic orbits embedded in the chaotic orbit. In particular, the chaotic saddle (formed by the intersections between the manifolds) has a Cantor dust structure similar to the horseshoe set. Such fractal structures have observable consequences in open Hamiltonian systems of physical interest, like the motion of charged particles in a magnetic field under the influence of electrostatic drift waves of different frequencies and wave numbers. In this case, we analyzed the presence of fractal structures in the so-called exit basins, which are the sets of initial conditions leading to an escaping orbit through some specified exit. The boundary between two escaping basins has shown to be a fractal curve through direct computation of its box-counting dimension, showing a value close to the phase space dimension, which means a highly convoluted curve. This fact leads, as a consequence, to a final-state uncertainty, i.e. once the initial condition is determined within a given uncertainty, it turns to be increasingly difficult to know for sure to which exit the ensuing orbit asymptotes to. We verified this fact also by computing the basin entropy, which is a novel measure for the degree of uncertainty related to fractal exit basin boundaries. Our results are not restricted to this particular physical system though, and are quite often observed in other open Hamiltonian systems as well.

Acknowledgments

This work has received the partial financial support from the following Brazilian government agencies: CNPq, CAPES and FAPESP (Processo 2011/19296-1). We would like to acknowledge useful discussions with Prof. Miguel Sanjuán (Madrid).

References

- [1] S. Bleher, C. Grebogi, E. Ott, and R. Brown, *Phys. Rev. A* **38** (1988) 930.
- [2] S. W. McDonald, C. Grebogi, E. Ott, and J. A. Yorke, *Physica D* **17** (1985) 125.
- [3] J. Aguirre, R. L. Viana, and M. A. F. Sanjuán, *Rev. Mod. Phys.* **81** (2009) 333.
- [4] G. Contopoulos, *Astron. Astrophysics* **231** (1990) 41.
- [5] G. Contopoulos, H. E. Kandrup and D. Kauffman, *Physica D* **64** (1993) 310.
- [6] J. Aguirre, J. C. Vallejo, and M. A. F. Sanjuán, *Phys. Rev. E* **64** (2001) 066208.
- [7] E. C. da Silva, I. L. Caldas, R. L. Viana, and M. A. F. Sanjuán, *Phys. Plasmas* **9** (2002) 4917.
- [8] J. S. E. Portela, I. L. Caldas, R. L. Viana and M. A. F. Sanjuán, *Int. J. Bifurcat. Chaos* **17** (2007) 4067.
- [9] W. Horton, *Plas. Phys. Contr. Fusion* **27** (1985) 937.
- [10] W. Horton, *Turbulent transport in magnetized plasmas* (World Scientific, Singapore, 2012)
- [11] A. C. Mathias, R. L. Viana, T. Kroetz, and I. L. Caldas, *Physica A* **469** (2017) 681.
- [12] R. K. W. Roeder, B. I. Rapoport, and T. E. Evans, *Phys. Plasmas* **10** (2003) 3796.
- [13] A. Daza, A. Wagemakers, B. Georgeot, D. Guéry-Odelin, and M. A. F. Sanjuán, *Sci. Rep.* **6** (2016) 3416.
- [14] G. Schmidt, *Physics of high-temperature plasmas* (Academic Press, New York, 1979).
- [15] F. A. Marcus, I. L. Caldas, Z. O. Guimarães-Filho, P. J. Morrison, W. Horton, Yu. K. Kuznetsov, and I. C. Nascimento, *Phys. Plasmas* **15** (2008) 112304